ENGINEERING

Toward a more sustainable mining future with electrokinetic in situ leaching

Evelien Martens[1,2], Henning Prommer[1,3]*, Riccardo Sprocati[4], Jing Sun[1,3,5], Xianwen Dai[6], Rich Crane[7], James Jamieson[1,3], Pablo Ortega Tong[1,3], Massimo Rolle[4], Andy Fourie[2]

Metals are currently almost exclusively extracted from their ore via physical excavation. This energy-intensive process dictates that metal mining remains among the foremost CO_2 emitters and mine waste is the single largest waste form by mass. We propose a new approach, electrokinetic in situ leaching (EK-ISL), and demonstrate its applicability for a Cu-bearing sulfidic porphyry ore. In laboratory-scale experiments, Cu recovery was rapid (up to 57 weight % after 94 days) despite low ore hydraulic conductivity (permeability = 6.1 mD; porosity = 10.6%). Multi-physics numerical model simulations confirm the feasibility of EK-ISL at the field scale. This new approach to mining is therefore poised to spearhead a new paradigm of metal recovery from currently inaccessible ore bodies with a markedly reduced environmental footprint.

INTRODUCTION

Industrial-scale metal and metalloid (hereafter metal) mining can be traced back several thousand years and marked the beginning of the Bronze Age (1). Mining technology has since undergone transformative change, both in terms of our ability to mine at scale and autonomously. Throughout this time, one fundamental component has remained constant: Mining activities have almost exclusively occurred via physical excavation, i.e., the process of physically removing solid ore-bearing minerals from the subsurface. This remains true today; such processes are responsible for more than 99 weight % (wt %) of all metals extracted from Earth each year (2). This requirement to haul ore to the surface dictates that large volumes of overburden must first be excavated, transported, and safely disposed. The ore then invariably requires removal of gangue material, often representing >99 wt %. The process results in the generation of inexorably large quantities of solid waste. Global estimates are of the order of 100 Gt per year (3), substantially larger than any other anthropogenic waste form and estimated to be several times more than the natural riverine transport of sediment to our oceans (4). Such metal recovery is also intrinsically energy intensive; the mining industry is among the most important individual contributors to the climate emergency (4). It is estimated that in 2018, greenhouse gas (GHG) emissions associated with primary mineral and metal production amounted to 3.6×10^{12} kg of CO_2 (excluding energy carriers, such as coal and uranium, and mineral aggregates), which was equivalent to ~10% of the total annual energy-related GHG emissions (5). Within this, copper (Cu) mining and refining were among the most intensive GHG emitters with approximately 6×10^{10} kg of CO_2 released (4). The hauling and storage of vast quantities of geological material often result in human, ecological,

and financial catastrophes, for example, the collapse of underground mines or tailings dams (6). Major tailings dam failures in the past decade include the 2019 Feijão dam disaster (Brazil; Fe ore, 32 million to 80 million m^3 tailings released; ≥237 deaths) (7), the 2015 Fundão dam disaster (Fe ore, 32 million to 60 million m^3 tailings released; ≥19 deaths) (8, 9), the 2019 Cobriza dam failure (Peru; Cu ore, 67,488 m^3 tailings released over 41,574 m^2) (10), and the 2018 Cadia dam failure (Australia; Au-Cu ore, 1.3 million m^3 tailings released and contained by southern dam) (11).

Cu currently plays a crucial role in our concurrent low-carbon energy transition; it is also used in a wide range of products and materials across industry and society (12). In recent years, Cu demand has burgeoned and has been predicted to increase by a further 275 to 350% by 2050 (13). During the past decade, there has been a major decline in the discovery of shallow (e.g., <100 m cover depth) Cu ore deposits while the average ore cutoff grade has also decreased by ~25% (14). For example, many Cu deposits currently deemed "Tier 1", such as the Pebble East giant copper-gold deposit in Alaska (USA) (15) and the deeper ore zones at the Escondida porphyry Cu deposit in Chile (16), are buried by hundreds of meters of overburden. Under these circumstances, conventional Cu mining becomes increasingly challenging because of the necessity to remove, process, and store large quantities of waste rock. Moreover, the economic viability of processing such diminishing grade material relies on a continual improvement in the efficiency of mining technologies and/or the economy of scale, i.e., the use of large infrastructure to deal with high throughput (17), using more energy, water, and land per unit mass of extracted Cu (5). Similar considerations also apply for many other commodities. Consequently, the current mining paradigm can be considered inherently unsustainable, and there is a recognized need for the development of new approaches for more sustainable exploitation of known but currently unviable metal deposits (18).

Here, we propose a new approach, electrokinetic in situ leaching (EK-ISL), which combines two existing technologies: (i) in situ leaching (ISL), which comprises the application of a lixiviant to selectively dissolve target metal(s) from their ore without removal of its host matrix, i.e., without excavation, and (ii) electrokinetics (EK), which comprises the application of a targeted electric field to control and accelerate transport (via electromigration) of the lixiviant

[1]School of Earth Sciences, University of Western Australia, Crawley, WA 6009, Australia. [2]Department of Civil, Environmental and Mining Engineering, University of Western Australia, Crawley, WA 6009, Australia. [3]CSIRO Land and Water, Private Bag 5, Wembley, WA 6913, Australia. [4]Department of Environmental Engineering, Technical University of Denmark, Bygningstorvet, Building 115, Kgs. Lyngby 2800, Denmark. [5]State Key Laboratory of Environmental Geochemistry, Institute of Geochemistry, Chinese Academy of Sciences, Guiyang 550081, China. [6]CSIRO Mineral Resources, Australian Minerals Research Centre, 7 Conlon St, Waterford, WA 6152, Australia. [7]Camborne School of Mines, College of Engineering, Mathematics and Physical Sciences, University of Exeter, Penryn, Cornwall TR10 9FE, UK.
*Corresponding author. Email: henning.prommer@csiro.au

and/or dissolved target metal(s) within the subsurface. EK is a relatively mature technology that has been applied in several fields of engineering, including metal recovery from fly ash, wastewater sludge, soils, and mine tailings materials (19–22). Its application to recover metals from intact hard rock bodies (e.g., primary ore deposits), however, is novel. Here, electrodes of opposite polarity are placed either within, or surrounding the ore, with cation migration directed toward the cathode(s) and anion migration toward the anode(s). The lixiviant is introduced via an external source reservoir and leached metals are collected from a target reservoir, which contains electrode(s) exhibiting opposite charge to the target metal-bearing ion. This setup (Fig. 1) allows for a precise control over the transport of both the lixiviant and the dissolved target metal(s) within the ore body.

As solute transport occurs via electromigration, this enables a relatively rapid movement of ions through low hydraulic conductivity media (23), thus circumventing the need for permeability enhancement techniques, such as hydraulic fracturing. The dependence of electromigration rates on tortuosity instead of the hydraulic conductivity promotes a more uniform delivery of the lixiviant to the target metal(s) rather than being limited to specific preferential flow paths that might host only a small fraction of the total grade. This is a transformative benefit given the tight (typical hydraulic conductivity $< 10^{-7}$ m/s) and heterogeneous nature of most ore deposits, which currently renders many conventional ISL opportunities unviable and environmentally hazardous to exploit.

EK-ISL is applicable for the hypogene zone of Cu porphyry deposits where the ore is usually hosted in the deeper zones of the porphyries, i.e., below the water table, as Cu sulfide with a typical grade of 0.5 to 1.5 wt %. These deposits comprise approximately 75% of current global copper reserves (24). In addition, it is thermodynamically viable to leach Cu at ambient temperature and pressure using relatively environmentally benign lixiviants, such as ferric chloride ($FeCl_3$). Porphyry Cu is typically hosted in fractured rocks that are commonly crosscut by quartz veins, with the majority of the Cu located along veins or disseminated throughout the surrounding rock mass (25). Under these circumstances, conventional ISL is considered unsuitable because of the prevalence of preferential flow, which would allow only a small proportion of the ore body to be accessed by the lixiviant. This limitation was evident, for example, in the Casa Grande porphyry "conventional" Cu ISL operation in Arizona (USA), where analysis of postleach drill cores revealed that a large fraction of the ore body was not exposed to the injected lixiviant (26).

RESULTS

Proof of concept of Cu recovery via EK-ISL

Laboratory-scale experiments (Fig. 2A) and process-based numerical modeling were used to assess the feasibility and scalability of EK-ISL for Cu extraction from sulfidic porphyry ore. Initial experiments were conducted using a synthetic Cu ore consisting of a homogenized mixture of quartz (80 wt % SiO_2, <75 μm) and chalcopyrite ($CuFeS_2$) (29 wt % Cu, <120 μm) powder (Tables 1 and 2). A 15.0 V direct current (DC) was applied over the length of the 96-mm-long reservoir hosting the synthetic ore mixture, and 0.5 M $FeCl_3$ was used as the lixiviant (Fig. 2, B to D). This resulted in the electromigration of Fe^{3+} (derived from the lixiviant) from the source reservoir into the Cu-bearing ore, wherein Cu dissolution occurred. Dissolved Cu, predominantly as Cu^{2+}, was then transported into the cathodic target reservoir and measured using atomic absorption spectroscopy (AAS). Our process-based numerical simulations capture the experimental observations, which show that Cu recovery occurred rapidly within the first 3 to 4 days, followed by a slower phase (Fig. 2D). This is typical for Cu leaching operations and can be attributed to the passivation of chalcopyrite surfaces with elemental sulfur (S^0) and/or low-pH stable iron hydroxide phases (e.g., jarosite) precipitates (27).

Subsequent experiments comprised the use of an intact sulfidic porphyry Cu ore drill core sample [8.6 wt % Cu, determined by inductively coupled plasma optical emission spectrometry (ICP-OES) following borate fusion] with a diameter and length of 38 and 40 mm, respectively. Quantitative x-ray diffraction (QXRD) for subsamples identified chalcopyrite (18.2 wt %) and covellite (CuS, 2.6 wt %)
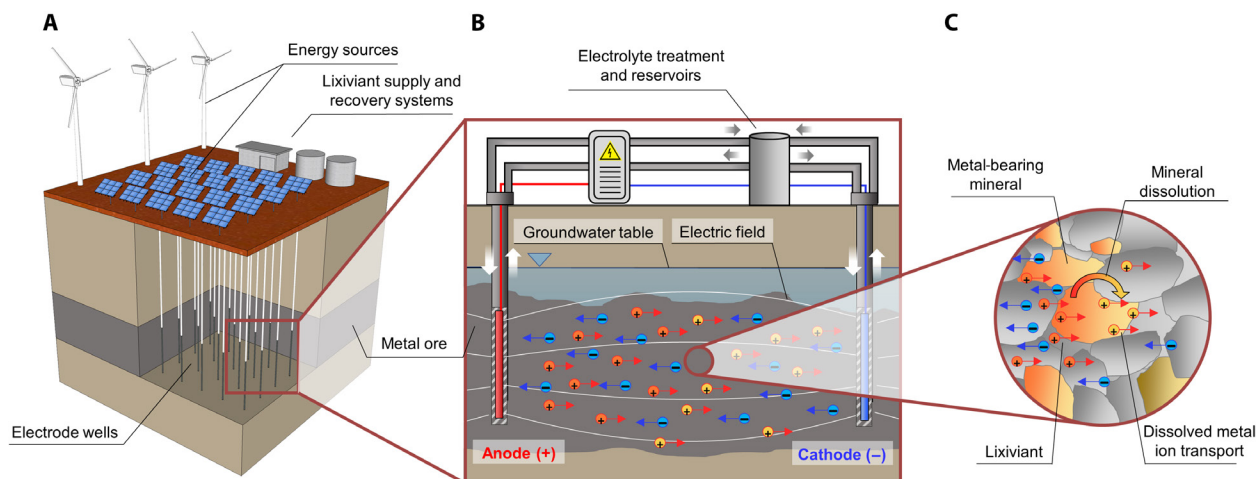
Fig. 1. Schematic illustration of metal extraction from a subsurface ore body via EK-ISL. (**A**) 3D isometric view of an industrial-scale EK-ISL operation, including potential electrode configuration, above-ground energy source, lixiviant supply and recovery reservoirs, and metal recovery treatment facility. (**B**) Cross-sectional view of the ore interface between an individual anode and cathode. (**C**) Conceptual illustration of principal hydrogeochemical reactions between the lixiviant and the ore material when subjected to EK-driven electromigration.
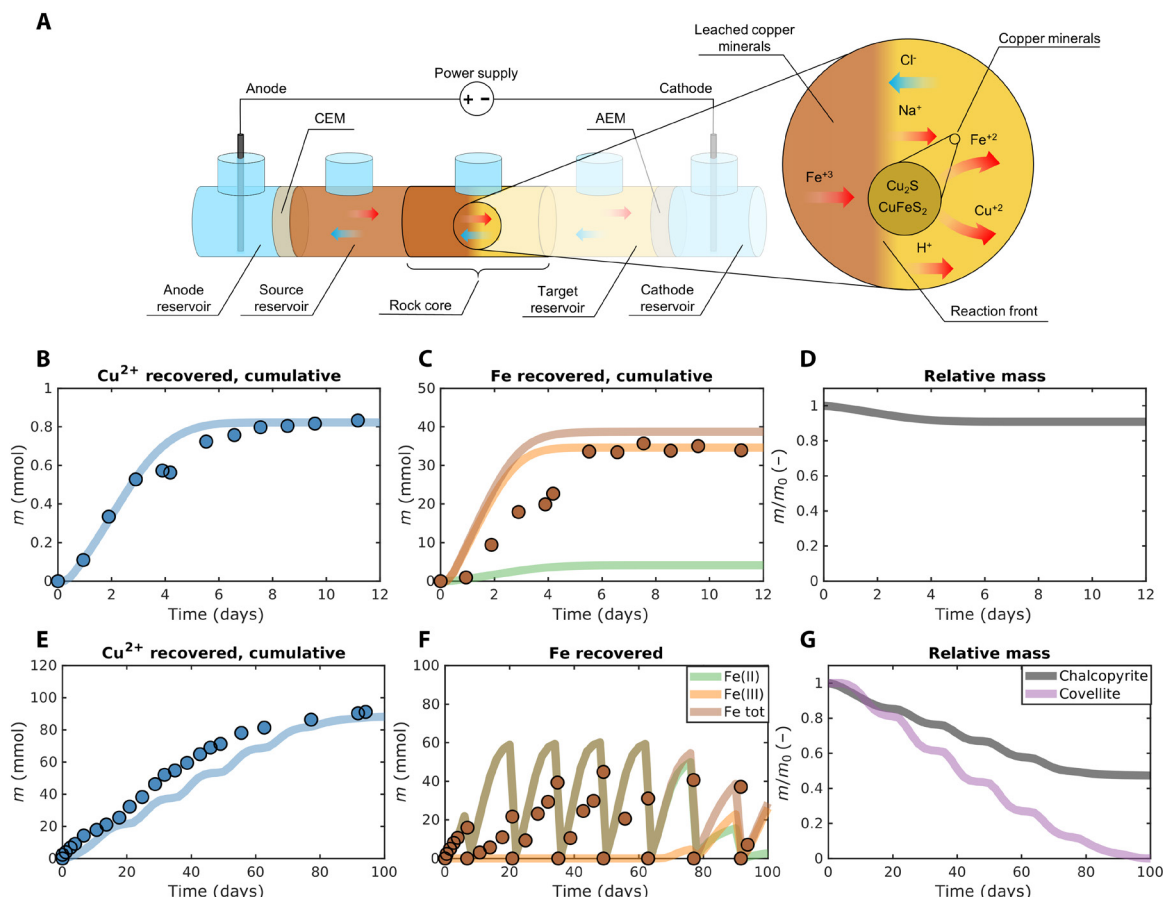
Fig. 2. Experimental setup and key results. (**A**) Illustration of experimental setup for EK-ISL of both synthetic and intact ore samples. CEM and AEM refer to cation and anion exchange membrane, respectively. The distance between anode and cathode was 0.57 m (synthetic ore) and 0.48 m (intact ore), respectively. Results of the laboratory-scale leaching experiments using (**B** to **D**) 0.5 M $FeCl_3$ and synthetic ore (quartz and chalcopyrite powder mixture, containing 9.15 mmol chalcopyrite) and (**E** to **G**) an intact ore sample composed of 75, 21, and 4 wt % of total Cu content present as chalcopyrite, covellite, and chalcocite, respectively. Symbols represent the measured experimental data taken from the target reservoir and the solid lines represent the results of the process-based model. Chalcocite was not considered in the model simulations because of its comparably small initial Cu mass fraction.

Table 1. QXRD analysis of the chalcopyrite powder. Cu minerals are highlighted in blue.

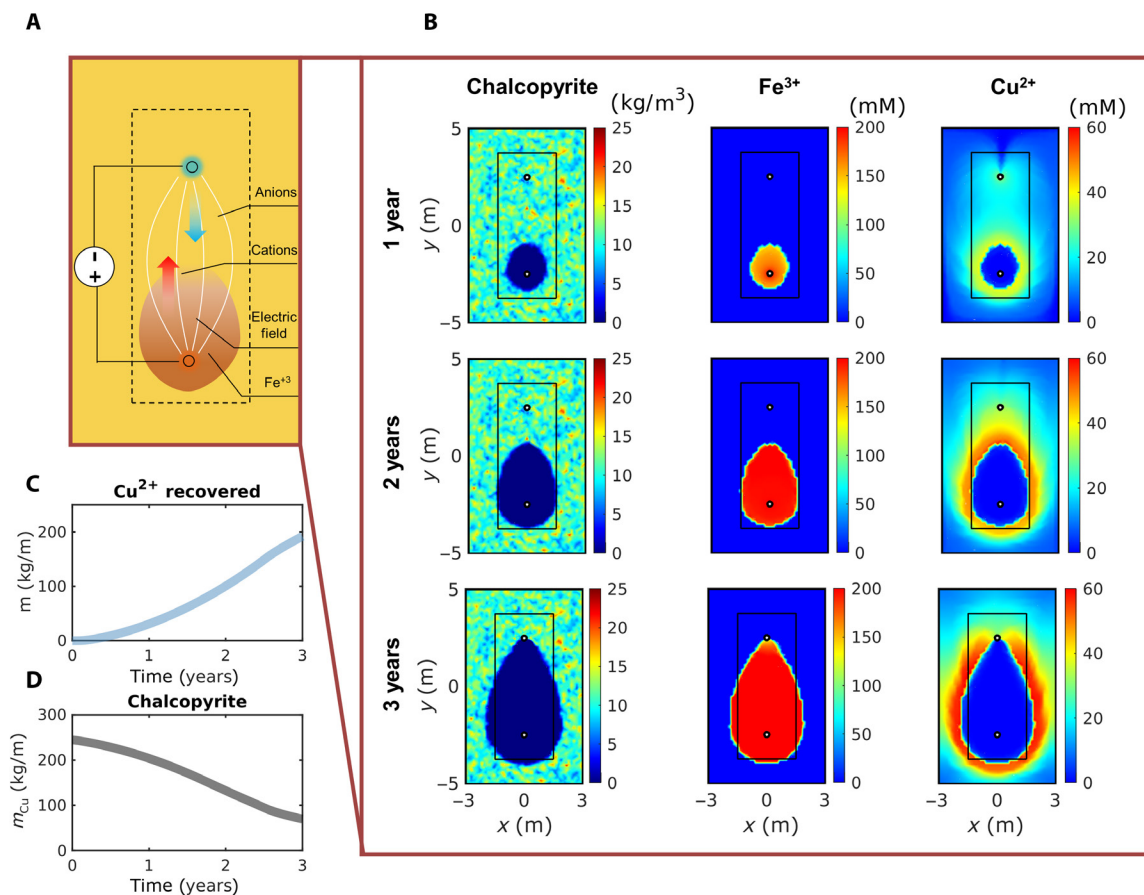| Mineral	Ideal formula	Content (wt %)
Kaolinite	$Al_2Si_2O_5(OH)_4$	1.2
Talc	$Mg_3(Si_2O_5)_2(OH)_2$	0.5
Jarosite	$(Na, K, H_3O^+)(Fe,Al)_3(OH)_6(SO_4)_2$	0.7
Illite	$K_{0.6}(H_3O)_{0.4}Al_{1.3}Mg_{0.3}Fe^{2+}_{0.1}Si_{3.5}O_{10}(OH)_2 \cdot (H_2O)$	0.8
Vermiculite	$Al_{10}Fe_2H_{80}Mg_{22}O_{124}Si_{22}$	0.3
Melanterite	$(Fe, Cu, Zn)SO_4 \cdot 7H_2O$	1.7
Apatite	$Ca_{10}(PO_4)_6(OH)_2$	8.1
Quartz	SiO_2	1.7
Pyrite	FeS_2	0.3
Chalcopyrite	$CuFeS_2$	84.6

Fig. 3. Numerical model setup and key results. (**A**) Schematic illustration of the EK-ISL design for the field-scale model. (**B**) Reactive transport simulation results for field-scale Cu recovery via EK-ISL assuming a 500 V difference between electrodes, a 5 m spacing between electrodes, and an 11 kg m^{-3} average Cu concentration within the ore. (**C**) Model simulation results for the cumulative Cu recovery during EK-ISL. (**D**) Chalcopyrite mass within the defined control domain [black rectangles indicated in (B)].

as the main Cu-bearing minerals, with a minor quantity of chalcocite (Cu$_2$S) (0.8 wt %) (Table 3 and fig. S1). This correlates to 75, 21, and 4 wt % of the total Cu content present as chalcopyrite, covellite, and chalcocite, respectively (Tables 3 and 4). Nuclear magnetic resonance (NMR) determined the ore to exhibit a porosity and permeability of 10.6% and 6.1 millidarcys (mD), respectively. A 7.0 V DC voltage was applied, which resulted in an estimated potential drop of 5.0 V between either end of the core, yielding a maximal voltage gradient of 1.75 V/cm, similar to what is typically applied during EK-based soil remediation (28–31). On the basis of solution compositions determined by AAS and ICP-OES, 57 wt % of Cu was recovered from its ore over 94 days (Fig. 2, E to G). Of the totally recovered Cu, 80 wt % (equivalent to 4.2 g Cu) was recovered within the first 50 days at a relatively constant rate. After this phase, the recovery rate of Cu gradually decreased.

QXRD on the postleaching material identified that the amount of chalcopyrite had decreased to 7.6 wt % during EK-ISL and that all the covellite and chalcocite has been successfully leached (Table 3). The recorded electric current decreased over the first 10 days from approximately 110 to 10 mA, consistent with temporary secondary mineral formation and associated blocking and/or narrowing of pores (21, 32). This phase was followed by a period of recovery, which suggests pore widening, most likely due to mineral dissolution (21, 32), to a final and relatively stable value of approximately 35 mA.

In addition to the changes in chalcocite/covellite concentrations, QXRD indicated that 3.0 wt % pyrite (FeS$_2$) underwent dissolution during the EK-ISL process, while S^0 was the only newly formed mineral (Table 3). Analysis of dissolved elemental concentrations within the source and target reservoirs using ICP-OES determined the most common species present as those originating from Cu minerals (Fe, S, and Cu), indicating that minimal gangue dissolution had occurred (Table 5). This is also corroborated by zero or minor changes between the pre- and postleaching ore material of total elemental concentrations of silica and potassium that would otherwise indicate dissolution of gangue aluminosilicates (Table 4) and the relatively similar pH values in both the source and the target reservoir solutions (fig. S2).

Evidence for the feasibility of EK-ISL at the field scale

Multiphysics numerical model simulations were used to upscale the experimental results to assess (i) the feasibility of EK-ISL to be used for Cu recovery in larger domains and (ii) the likely time scale required for recovery. A simple dipole EK-ISL configuration (Fig. 3A) was applied, which comprised a single cathode and a single anode spaced 5 m apart in a two-dimensional (2D) domain with an extent of 6 m by 10 m. The physical and hydrogeochemical properties of the ore were inferred from our process-based numerical model simulations of the laboratory-scale experiments (see the Supplementary

Table 2. Total element concentrations in the pure copper mineral powder (chalcopyrite) used in the synthetic ore experiments analyzed using ICP-OES following borate fusion method (lithium borate flux).

Element	Al	Ca	Fe	Mg	Si	Cu	S	K	Ni	Cr	Mn	Ti	Zn	As	Ba	Co	P	Na	C	Cl
%	0.12	3.2	26.8	0.25	1.11	29.1	30.1	0	0.04	0	0	0	0.010	0.005	0	0.021	1.38	0	0.01	0.03

Table 3. QXRD analysis of the copper ore offcuts (not affected by EK-ISL treatment) and the ore sample after EK-ISL treatment. *Cu minerals. The determined values after EK-ISL have been corrected for the mass loss due to the leaching process.

Mineral	Ideal formula	Mass (wt %)[#]	
		Offcuts (untreated)	Sample after EK-ISL
K-alunite	$K(Al, Fe)^{3+}_3(OH)_6(SO_4)_2$	3.5	5.1
Siderotil	$FeSO_4.5H_2O$	1.1	0.5
Na-jarosite	$Na(Al, Fe)^{3+}_3(OH)_6(SO_4)_2$	1.1	0.7
Pyrophyllite	$H_2Al_2O_{12}Si_4$	10.1	4.4
Quartz	SiO_2	55.3	60.4
Pyrite	FeS_2	5.5	2.5
Chalcopyrite*	$CuFeS_2$	18.2	7.6
Chalcocite*	Cu_2S	0.8	1.3
Covellite*	CuS	2.6	0.0
Molybdenite	MoS_2	0.3	0.4
Illite	$K_{0.6}(H_3O)_{0.4}Al_{1.3}Mg_{0.3}Fe^{2+}_{0.1}Si_{3.5}O_{10}(OH)_2 \cdot (H_2O)$	1.6	1.0
Elemental sulfur	S	0.0	1.9

Table 4. Total element concentrations of crushed and milled offcuts (no EK-ISL treatment) and the ore sample after EK-ISL treatment using ICP-OES following borate fusion method (lithium borate flux). The mass balance for Cu indicates Cu leached + residual Cu retained in the ore, as determined by total acid digestion = 9.26 g; initial Cu mass estimated by QXRD analysis for offcuts of the same drill core sample = 10.85 g. The values determined after EK-ISL have been corrected for the mass loss due to the leaching process.

Sample	Concentration (%)									
	Al	Ca	Fe	Mg	Au	Mo	Si	Cu	K	S
Sample offcuts (untreated)	5.45	0.05	9.48	0.03	0.01	0.07	26.20	8.24	0.72	13.40
Sample after EK-ISL	5.12	0.05	4.60	0.01	0.01	0.11	26.20	2.97	0.68	10.28

Table 5. ICP-OES data for selected solution samples in the EK-ISL test on the rock sample. T6 = target after 6.9 days, T10 and S10 = target and source after 20.9 days, T20 and S20 = target and source after 49.1 days.

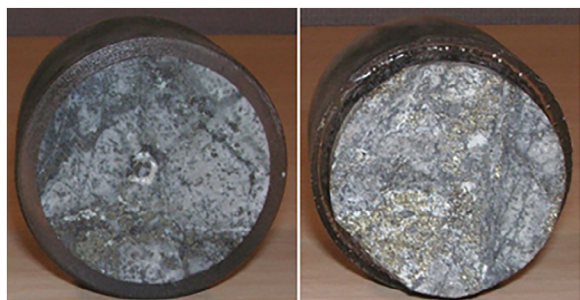| Sample	Concentration (mg/liter)										
	Al	Ca	Fe	Mg	Au	Mo	Si	Cu	K	S	TC
T6	8.25	157	1996	5.37	0.385	6.19	1.35	2126	2.04	715	8.08
T10	13.8	90.9	2620	4.91	0.330	14.9	2.08	2748	4.12	507	8.68
T20	3.60	53.0	5127	<0.2	0.369	3.88	1.69	2241	0.675	17.1	5.60
S10	1.44	42.1	21,618	0.380	0.539	<0.2	3.79	191	2.78	405	13.4
S20	8.49	9.57	22,544	<0.2	0.766	0.516	1.16	568	2.37	328	8.28

Fig. 4. Four-centimeter-long copper ore sample (3.8 cm in diameter) before the start of the experiment. Source-facing side (left) and target-facing side (right). The ore sample was molded in epoxy resin to a thickness of ~1 cm to fit in the experimental apparatus.

Materials for full details). The Cu ore was assumed to contain heterogeneously distributed chalcopyrite with an overall Cu grade of 0.44 wt %, i.e., within the 0.3 to 0.9 wt % range, which comprises the vast majority of currently viable Cu deposits worldwide (33). No gangue aluminosilicates were considered in the reaction network as in our laboratory experiments, and no evidence for aluminosilicate dissolution was found. The model framework that we used for the simulations considers the integrated description of ionic transport via electromigration, Coulombic interactions between transported species, and kinetically controlled geochemical reactions (34).

Figure 3 illustrates the key results of the model simulations, including the spatial and temporal evolution of the major reactants and both cumulative Cu recovery over the 3-year simulation period (Fig. 3C) and the corresponding chalcopyrite mass within a selected control domain (Fig. 3D). Induced by aqueous Fe^{3+} that is transported via electromigration from the anode to the cathode, leaching of chalcopyrite evolves successively from the anode toward the cathode (Fig. 3B). The shape of the migrating Fe^{3+} plume mirrors the zone in which chalcopyrite is depleted. The position of the reaction front and its sharpness are the result of chalcopyrite dissolution being controlled by the supply of Fe^{3+} rather than by reaction kinetics (Fig. 3B). This Fe^{3+} mass flux is predominantly controlled by the applied electric potential gradient, i.e., the voltage that is applied at the anode/cathode pair (see the Supplementary Materials for additional details). Dissolved Cu^{2+} is transported by electromigration toward the cathode with concentrations highest at the fringe of the chalcopyrite-depleted zone, i.e., the reaction front (Fig. 3B). This behavior can be attributed to the electrostatic interactions that strongly influence the transport of ions and thus exert a key control on EK-ISL efficiency (35). The model results show that ~70 wt % of the initial grade (Fig. 3J) was recovered over the 3-year simulation period (Fig. 3D) at a relatively constant rate.

DISCUSSION
Our experimental and process-based numerical modeling results jointly indicate that EK-ISL is an effective and scalable approach for Cu recovery from hard rock deposits within a viable time scale. This is supported by earlier studies that demonstrate that electromigration rates of ionic species through intact crystalline rocks can be several orders of magnitude faster than molecular diffusion (36–38). EK-ISL–driven electromigration of ions is governed by the location of

cathode and anode arrays, largely independent of the prevailing subsurface hydrogeological structure. A high degree of control can therefore be exerted over solute migration pathways. Given that rock masses in which diffusion is the dominant transport mechanism will be the main target of EK-ISL, this also implies that once the mining process is terminated and the electric current is no longer applied, solute migration rates will be extremely low and the risk of offsite migration of any hazardous solutions is markedly reduced. This is a notable advantage over conventional ISL, for which flow control and offsite migration are often cited as key technical barriers preventing the social license to operate (25).

EK-ISL will likely be best suited for ore bodies located below the groundwater table as electromigration rapidly becomes inefficient with declining water saturation (23). For Cu mining in porphyry deposits, such conditions mostly occur in chalcopyrite– and bornite (Cu_5FeS_4)–dominated ore in the deeper zone and the enriched zone just above it, which typically consists of sulfides at higher-sulfidation states, such as chalcocite and covellite (CuS) (24). Targeting these deeper, anoxic zones is advantageous (for acid-bearing lixiviants) as they typically have a much lower abundance of carbonates that would otherwise consume such lixiviant acidity before the pH is sufficiently lowered to allow the Cu mobilization (39).

Maintaining solubility of the Fe^{3+}-bearing lixiviant is one potential challenge that will likely need to be considered at field scale. Figure S2 shows that establishment of strongly acidic conditions (i.e., pH < 2) throughout the treatment zone was maintained. It is conceivable, however, that when scaling up the EK-ISL process, heterogeneity within the ore deposit, including the presence of localized pH buffering gangue minerals, could cause precipitation of the lixiviant, which could result in pore clogging and an associated decline in Cu recovery rates. Further research in this area is needed to confirm under what hydrogeochemical conditions and/or types of ore deposit(s) this may occur. The extent of surface passivation of Cu-bearing minerals is another area to explore at field scale. This is also dependent on the prevailing geochemical conditions (i.e., more prevalent at pH > 2) but could potentially be overcome by modifying the EK field (e.g., pulsating or alternating the EK field) to provide the necessary activity to cleave such secondary precipitates away from the Cu-bearing mineral surfaces.

EK-ISL is also applicable for a broader range of leachable metals and deposit types worldwide. Besides leaching of Au, which we previously demonstrated at the laboratory scale (40), and Cu here, EK-ISL is also potentially applicable for a wide range of minerals containing silver, zinc, cadmium, lead, manganese, lithium, molybdenum, selenium, vanadium, scandium, yttrium, rare earth elements, indium, beryllium, chromium, gallium, nickel, and cobalt. Furthermore, there is great potential for artisanal, small-scale, and/or decentralized mining applications because of the ability to leach high-grade and small-scale, but currently unconventional, deposits (such as narrow vein deposits) largely independent of over- and interburden. Given the fact that EK-ISL can enable metal recovery with markedly reduced disturbance of the surface environment, it is also amenable for regions of increased population and/or infrastructure density, such as Europe, in addition to regions that exhibit high ecological sensitivity, cultural, and/or aesthetic value. In many mining regions, especially arid environments such as Chile and Australia, the majority of the electric power requirements can be provided by (decentralized) solar energy or, alternatively, by wind power. EK-ISL therefore bears a tremendous potential

for us to step beyond the current paradigm of metal extraction from the subsurface via physical excavation toward a more environmentally friendly mining future. Humankind is currently in the midst of a dual environmental crisis of resource scarcity and waste overload. EK-ISL, where applicable, could lead to a more sustainable exploitation of currently unviable metal resources while markedly reducing waste generation. Such radical changes are urgently required for us to prevent concurrent environmental and human health impacts from conventional mining and waste storage practices, while also diversifying and upscaling supply chains of a number of metals that are urgently required for our transition to a low-carbon economy.

To date, many of the true costs of mining via excavation have been barely or inadequately considered. Any forthcoming economic evaluation of EK-ISL will need to more holistically take into account the reduced capital cost, reduced environmental footprint, and increased social acceptance, thereby overcoming conventional cost calculations that overemphasize rapid extraction of high-grade resources and underrepresented environmental values.

MATERIALS AND METHODS

Experiment with synthetic ore

A synthetic ore sample was used to evaluate the principal feasibility of EK-ISL for Cu while limiting possible complications from both mineral and physical heterogeneity and interactions with gangue minerals. A Cu mineral typical to the deeper zones, i.e., chalcopyrite, was selected for the "synthetic ore". The synthetic ore sample was prepared by homogenizing finely crushed chalcopyrite specimen into (nonreactive) quartz powder (80 wt % SiO_2, <75 μm).

The chalcopyrite specimen was obtained from Geo Discoveries (Australia) and milled to powder (<120 μm) before analytical characterization. On the basis of QXRD analysis, the specimen contained 84.6% chalcopyrite, with apatite $[Ca_{10}(PO_4)_6(OH)_2]$ making up most of the remaining mass (Table 1). Elemental composition of the specimen was determined by borate fusion followed by ICP-OES (model: Agilent Technologies 5110 ICP-OES), which showed that Cu content in the specimen was 29.1% (Table 2). On the basis of mass balance calculation, chalcopyrite accounted for 100% of the Cu.

Acidic ferric chloride, which can induce the oxidative dissolution of sulfides, was chosen as the lixiviant in this study (41–43). $FeCl_3$ (0.5 M, 28 g/liter Fe) in 0.2 M HCl was used for all the experiments. All chemicals used for lixiviant preparation throughout this study were of reagent grade or higher purity. The Milli-Q water used here had a resistivity of 18.2 megohm cm.

On the basis of a previously published design (40, 44, 45), a laboratory-scale EK-ISL apparatus was constructed to carry out 1D experiments (Fig. 2A). The apparatus consisted of five reservoirs. The middle reservoir contained the ore sample to be leached, with the source reservoir, representing an injection well and the target reservoir, representing an extraction well on either side of the ore-bearing reservoir. The lixiviant was added into the source reservoir, and a solution with an initial composition of 0.3 M NaCl in 0.2 M HCl (corresponding ionic strength of ~0.5 M) was added into the target reservoir. The electrodes were housed in the outer two electrode reservoirs and connected to a DC power supply. The electrodes used were mixed metal oxide–coated titanium electrodes from McCoy Engineering (Osborne Park, Australia). The two outer reservoirs contained electrolytic solutions of 100 mM NaCl as catholyte and 50 mM Na_2SO_4 as anolyte. The cathode and anode

reservoirs were separated from the inner reservoirs by an anion and a cation exchange membrane, respectively. Both membranes were obtained from Membranes International Inc. (Ringwood, USA). Ionic membranes isolated the electrolyte reservoirs from the rest of the system, limiting the metal leaching process and transport within the three inner reservoirs, while still allowing for electrical flow. Under an electric field, the cationic lixiviant components H^+ and Fe^{3+} would move from the source reservoir to the target reservoir through the ore zone. Leached Cu^{2+} and other cations would move in the same direction. The use of the anion exchange membrane prohibited metal cations moving into the cathode reservoir and resulted in the accumulation of metal cations within the target reservoir. The application of an electric field results in electrolysis of water at the anode and cathode (21). To compensate for the hydrogen (H^+) and hydroxyl (OH^-) ions generated at the anode and cathode, respectively, NaOH (4 M) and HCl (4 M) were manually added to the respective electrolyte reservoirs periodically.

For this experiment, the middle reservoir was filled with a homogeneous mixture of 360 g of silica powder and 2 g of chalcopyrite powder at 84.6% purity (equivalent Cu concentration of 586 mg), saturated with 0.137 liters of 100 mM NaCl. The synthetic ore sample was held in place by a fabric piece inserted between two plastic support structures on each side. The experiments with synthetic ore were run at a fixed voltage of 15 V, while the current could freely vary unless the system reached a maximum current of 220 mA, in which case a switch to a constant current with variable voltage was triggered automatically. Because frequent, manual addition of NaOH and HCl to the electrolyte reservoirs was required under high current setting, the voltage setting was sometimes adjusted from 15 to 7.5 V. The time and duration of the adjustments were recorded. As the driving force for electromigration was halved during the adjustments, the data from the EK-ISL experiments were reported as a function of "equivalent time under 15 V/220 mA setting" by assuming linearity, instead of real experimental time. The source and target reservoirs were sampled regularly during the experiments and analyzed for a suite of dissolved elements including Cu and Fe concentrations using AAS (model: Agilent Technologies, 200 series AA). The pH values within the source and target reservoir were also recorded regularly using a calibrated electrode (TPS WP-80 pH meter and TPS Double Junction pH electrode).

Experiments with intact ore sample

The intact ore sample originated from a porphyry copper deposit. A representative ore sample was selected from the deeper hypogene zone of this deposit, which is enriched with sulfides. A 4 cm long, 3.8-cm–internal diameter cylindrical subsample was drilled and used for the EK-ISL experiment (Fig. 4). On the basis of NMR measurement on an offcut of the ore sample, the intact ore sample had a porosity of 10.6% and a (low) permeability of 6.1 mD. Offcuts were crushed and milled to less than 5 μm and analyzed by QXRD and borate fusion followed by ICP-OES, respectively, for mineralogy and elemental composition. QXRD identified chalcopyrite, covellite, and chalcocite as the Cu-bearing minerals, with the amounts being 18.2, 2.6, and 0.8%, respectively (Table 3). On the basis of ICP-OES results, total Cu content in the ore was 8.24% (Table 4). Therefore, chalcopyrite, covellite, and chalcocite accounted for 75, 21, and 4% of the total Cu content of the ore, respectively.

Before the experiment, the drilled ore subsample was placed in 0.1 M NaCl under vacuum for 8 days and at atmospheric pressure

for another 17 days to saturate the pores with electrolyte and then placed in the middle reservoir of the EK-ISL apparatus (Fig. 2A). The EK-ISL experimental procedures for the intact ore were consistent with those applied for the synthetic ore unless mentioned otherwise. The experiment with the intact ore was operated under a constant voltage setting of 7 V, with only occasional short interruptions while the power was turned off, for example, while solutions were refreshed. These periods were deducted from the reported times. Therefore, the reported times correspond to the time elapsed under operation. Note, however, that the difference between the overall time and the time under operation is negligible (<24 hours). The FeCl$_3$-HCl lixiviant in the source reservoir was refreshed on days 21, 35, 49, 63, 77, and 92. On these days and additionally on day 7, the NaCl-HCl solution in the target reservoir was renewed to prevent precipitation due to accumulation of cations. The total duration of the EK-ISL experiment using the intact ore was 94 days, during which the source and target reservoirs were sampled regularly (2 ml) and analyzed for solution composition. The pH values and the electric current were regularly recorded using a calibrated handheld multimeter (TPS WP-80 pH meter and TPS Double Junction pH electrode). Once the experiment was complete, the postleaching ore sample was retrieved, crushed, and milled to less than 5 μm and subsequently analyzed using QXRD and borate fusion followed by ICP-OES and scanning electron microscope energy dispersive spectroscopy (SEM-EDS).

Process-based numerical model development

Numerical reactive transport models were set up to analyze and quantify the electromigration process through the intact ore coupled with the key geochemical processes that affect mineral oxidative dissolution and Cu transport. Reactive transport models of the synthetic chalcopyrite and real ore experiments were developed and calibrated against the experimental data. The developed model, including the reaction network used and reaction rate parameters, was subsequently extended to a 2D field-scale model.

In low-permeability porous media and in absence of groundwater flow, the flux of charged species in saturated conditions is governed by diffusive and electromigration fluxes as described with the Nernst-Planck equation

$$\boldsymbol{J}_i^{\text{Tot}} = \underbrace{-nD_i \nabla c_i}_{\boldsymbol{J}_i^{\text{Dif}}} \underbrace{-nD_i \frac{z_i F}{RT} c_i \nabla \Phi}_{\boldsymbol{J}_i^{\text{Mig}}} \tag{1}$$

where n (−) is the accessible porosity, D_i (m^2 s^{-1}) is the pore diffusion coefficient calculated as $D_i = D_i^{aq} \tau$ with D_i^{aq} (m^2 s^{-1}) being the aqueous diffusion coefficient and τ (−) being the tortuosity, ∇c_i (mol m^{-4}) is the concentration gradient, z_i (−) is the charge of the species i, F (C mol^{-1}) is the Faraday constant, R (J mol^{-1} K^{-1}) is the gas constant, T (K) is the temperature, c_i (mol m^{-3}) is the molar concentration, and $\nabla \Phi$ (V m^{-1}) is the electric potential gradient. In Eq. 1, $\boldsymbol{J}_i^{\text{Tot}}$ (mol m^{-2} s^{-1}) indicates the total flux of a species i, which is the sum of the diffusive flux $\boldsymbol{J}_i^{\text{Dif}}$ (mol m^{-2} s^{-1}) and the electromigration flux $\boldsymbol{J}_i^{\text{Mig}}$ (mol m^{-2} s^{-1}).

The governing multicomponent ionic transport equation is derived considering the mass balance

$$\frac{\partial (nc_i)}{\partial t} + \nabla \cdot \boldsymbol{J}_i^{\text{Tot}} = r_i \tag{2}$$

in which r_i (mol m^{-3} s^{-1}) is the source/sink term. The relation between charge density of the solution ρ_e (C m^{-3}) and electric field is described by Poisson's equation (46)

$$\nabla^2 \Phi = -\frac{F}{\varepsilon} \sum_{i=1}^{N} z_i c_i = -\frac{\rho_e}{\varepsilon} \tag{3}$$

where ε (F m^{-1}) is the dielectric constant of the porous medium and N is the number of charged species in solution. At the continuum scale, the net charge density in the system is zero (47, 48) and Eq. 3 accounts for the electroneutrality condition ($\sum_{i=1}^{N} z_i c_i = 0$).

The continuity condition in terms of charge is

$$F \sum_{i=1}^{N} z_i \frac{\partial (nc_i)}{\partial t} + \nabla \cdot \left(F \sum_{i=1}^{N} z_i \boldsymbol{J}_i^{\text{Tot}} \right) = F \sum_{i=1}^{N} z_i r_i \tag{4}$$
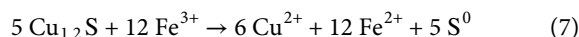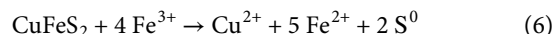
The EK transport of dissolved species in porous media can ultimately be described using the set of Eqs. 1 to 4, which constitutes the Nernst-Planck-Poisson equations (NPPE), including the respective conservation equations.

The change in concentration of the lixiviant and the dissolved metals in the reservoirs are modeled using the reservoir equation, which accounts for flushing and refills at specific times

$$\frac{\partial c_i}{\partial t} = (\pm \boldsymbol{J}_i^{\text{Tot}}) A / V - f_{\text{flu}} Q_{\text{flu}} c_i / V + f_{\text{ref}} Q_{\text{ref}} c_{i,\text{ref}} / V \tag{5}$$

where A (m^2) is the cross-sectional area of the reservoir, V (m^3) is the reservoir volume, and f_{flu} (−) and f_{ref} (−) are stepwise functions that regulate the time at which flushing and refill of electrolytes at the reservoirs are performed. Q_{flu} (m^3 s^{-1}) and Q_{ref} (m^3 s^{-1}) are the flow at which the reservoirs are flushed and refilled during the specified times. The positive or negative sign for the total fluxes in Eq. 5 indicates fluxes respectively entering or exiting the reservoir chamber.

The reaction network used in the simulations primarily considers the oxidative dissolution of copper sulfide minerals by ferric iron (Fe^{3+}). Mineral dissolution reactions for chalcopyrite and covellite (CuS) by dissolved Fe^{3+} are described as (41–43)

$$\text{CuFeS}_2 + 4\,\text{Fe}^{3+} \rightarrow \text{Cu}^{2+} + 5\,\text{Fe}^{2+} + 2\,\text{S}^0 \tag{6}$$

$$5\,\text{Cu}_{1.2}\text{S} + 12\,\text{Fe}^{3+} \rightarrow 6\,\text{Cu}^{2+} + 12\,\text{Fe}^{2+} + 5\,\text{S}^0 \tag{7}$$

In this study, we considered only the species that were identified to affect the key processes that were proceeding during the experiments, i.e., Na$^+$, Cl$^-$, Fe^{2+}, Fe^{3+}, Cu^{2+}, H$^+$, and OH$^-$ (diffusion coefficients provided in table S1). The considered solid phases were elemental sulfur and the Cu minerals chalcopyrite and covellite. The oxidative dissolution reactions were implemented as kinetically controlled reactions.

For chalcopyrite, the stoichiometry defined in Eq. 6 was used and the reaction rate expression was defined as (49)

$$r_{\text{cp}} = k_{\text{cp}} [\text{H}^+]^{0.8} [\text{Fe}^{3+}]^{0.42} e^{\left(\frac{-48,100}{RT} \right)} k_{\text{pas1}} \tag{8}$$

where r_{cp} (mol liter^{-1} s^{-1}) is the dissolution rate for chalcopyrite, k_{cp} (mol$^{-0.22}$ liter$^{0.22}$ s^{-1}) is the rate constant for chalcopyrite dissolution,

R is the gas constant (J mol^{-1} K^{-1}), and T (K) is the temperature. Passivation of chalcopyrite was suggested by the presence of elemental sulfur on the surface of leached chalcopyrite samples and the observation that diffusion through a product layer may slow down chalcopyrite dissolution (27, 50). This hypothesis was supported by postleaching SEM images of the ore sample, which indicated that the accumulation of elemental sulfur was associated with grains of chalcopyrite (fig. S3). Therefore, a passivation term k_{pas1} was added to Eq. 8 to account for sulfur precipitation, which decreases chalcopyrite dissolution rates over time

$$k_{pas1} = e^{(-a_{cp} \times [S^0])} \qquad (9)$$

where a_{cp} (mol^{-1} liter) is an empirical constant that relates chalcopyrite dissolution to the sulfur precipitation.

For natural or primary covellite, we used the stoichiometry in Eq. 7 and a reaction rate similar to Eq. 8

$$r_{pc} = k_{pc} \times [Fe^{3+}] \times e^{\left(\frac{-8948}{T}\right)} \times k_{pas2} \qquad (10)$$

where r_{pc} (mol liter^{-1} s^{-1}) is the dissolution rate for primary covellite and k_{pc} (s^{-1}) is the rate constant for primary covellite dissolution. A passivation term k_{pas2} as used in the chalcopyrite rate (Eqs. 8 and 9) was incorporated to account for the reduced dissolution rate of primary covellite during the buildup of S^0 [e.g., (51)].

Physical and chemical 2D isotropic heterogeneity were generated for the 2D field-scale model simulations, as shown in fig. S4. The spatial random field was generated with the Python package GSTools (52) using a truncated power law variogram. Values of the output raster file were normalized, and the resulting spatial field $\gamma(x, y)$ ranges from 0 to 1. The dimensions of γ have been scaled in order to be as wide as the largest dimension of the model domain.

Physical heterogeneity was implemented considering a tortuosity distribution according to the following expression

$$\tau = \tau_x(|1 - 0.8\,\gamma| + 0.1) \qquad (11)$$

where τ indicates a spatially variable tortuosity and τ_x is a constant. Porosity variations have been related with the tortuosity through Archie's law

$$F = a\,n^{-m} \qquad (12)$$

with $a = 1$ and $m = 0.85$, in which the formation factor F has been considered as representative of the (electric) tortuosity (53).

Mineral heterogeneity was implemented considering the following expression

$$c_m = c_x(|1 - 0.8\,\gamma| + 0.1) + c_x \qquad (13)$$

where c_x is a constant.

The resulting heterogeneous mineral distribution was then inserted into COMSOL, with all relevant model dimensions provided in table S6.

The reactive transport simulations were performed with the code NP-Phreeqc-EK, which couples COMSOL Multiphysics and PhreeqcRM (54) through a MATLAB LiveLink interface, as described in detail in (34, 35). The NP-Phreeqc-EK code solves the NPPE for conservative and reactive transport in multidimensional domains.

Modeling of laboratory experiments

Reactive transport models were developed and calibrated using data from two of the laboratory-scale EK-ISL experiments: (i) the synthetic chalcopyrite experiment and (ii) the intact copper ore experiment (tables S3 to S7). These initial model simulations provided the basis for determining the transport properties and kinetic parameters governing the oxidative dissolution reactions of Cu minerals contained within the ore (Table 3). Both models were implemented as 1D models, in which the length was defined by the length of the core sample. The electric potential gradient was applied at the two respective boundaries of the domain, and the voltage at the anode was assumed to be constant, calculated based on the ideal electric potential gradient applied in the experiment (125 V/m) and the length of the sample. The reservoirs were also implemented at the edges of the domain and the concentration of the species was regulated according to Eq. 5. The models did not include electrolysis reactions as the pH at the reservoirs was intermittently buffered. The initial concentration of Fe^{3+} at the reservoirs was considered as a fitting parameter, and the lower modeled concentration with respect to the experiment takes into account possible precipitation effects. For both the chalcopyrite and the ore experiment, the only adjustable transport parameter was the tortuosity. In addition, the rate coefficients for the dissolution reactions were adjusted during the model calibration. A list of all model input parameters is shown in Table 4.

Modeling of field-scale electrode pair configuration.

An electrode pair configuration was designed to illustrate the delivery over time of the lixiviant and the leaching of copper sulfide minerals in 2D domain with an extent of 6 m by 10 m (see Fig. 3).

The distance between electrodes was set to 5 m, and the system was operated under constant electric potential for a total duration of 3 years. An inner domain was considered to evaluate the evolution of the mineral mass over time, to reduce the influence of stagnant zones on the evaluation of the mass fluxes of lixiviant and Cu recovery. Further details characterizing the 2D model simulation are provided in tables S6 and S7. Boundary conditions at the electrodes were assumed to be constant, as it is envisaged that field application of EK-ISL would implement periodic recirculation of electrolytes with reservoirs housing the electrodes.

SUPPLEMENTARY MATERIALS

Supplementary material for this article is available at http://advances.sciencemag.org/cgi/content/full/7/18/eabf9971/DC1

REFERENCES AND NOTES

1. D. Killick, T. Fenn, Archaeometallurgy: The study of preindustrial mining and metallurgy. *Ann. Rev. Anthropol.* **41**, 559–575 (2012).
2. M. Seredkin, A. Zabolotsky, G. Jeffress, In situ recovery, an alternative to conventional methods of mining: Exploration, resource estimation, environmental issues, project evaluation and economics. *Ore Geol. Rev.* **79**, 500–514 (2016).
3. M. Tayebi-Khorami, M. Edraki, G. Corder, A. Golev, Re-thinking mining waste through an integrative approach led by circular economy aspirations. *Minerals* **9**, 286 (2019).
4. B. Lottermoser, *Mine Wastes* (Springer Berlin Heidelberg, 2010); http://link.springer.com/10.1007/978-3-642-12419-8.
5. M. Azadi, S. A. Northey, S. H. Ali, M. Edraki, Transparency on greenhouse gas emissions from mining to enable climate change mitigation. *Nat. Geosci.* **13**, 100–104 (2020).
6. A. Fourie, Reflections on recent tailings dam failures and how the application of burland's soil mechanics triangle concept may avert future failures. *Geotech. Eng.* **51**, 60–64 (2020).
7. P. K. Robertson, D. J. Williams, G. Ward Wilson, *Report of the Expert Panel on the Technical Causes of the Failure of Feijão Dam I* (2019); http://b1technicalinvestigation.com/report.html.

8. N. R. Morgenstern, S. G. Vick, C. B. Viotti, B. D. Watts, *Report on the Immediate Causes of the Failure of the Fundão Dam* (2016); http://fundaoinvestigation.com/the-report/.

9. K. Hudson-Edwards, Tackling mine wastes. *Science* **352**, 288–290 (2016).

10. Wood Mackenzie, *Cobriza Copper Mine Report* (2020); https://woodmac.com/reports/metals-cobriza-copper-mine-16202151.

11. Newcrest Mining, *Market Release. Expert Review of Cadia Tailings Facility* (2019); https://newcrest.com/sites/default/files/2019-10/190430_Market Release_Expert review of Cadia tailings facility completed_0.pdf.

12. O. Vidal, B. Goffé, N. Arndt, Metals for a low-carbon society. *Nat. Geosci.* **6**, 894–896 (2013).

13. A. Elshkaki, T. E. Graedel, L. Ciacci, B. K. Reck, Copper demand, supply, and associated energy use to 2050. *Glob. Environ. Chang.* **39**, 305–315 (2016).

14. G. Calvo, G. Mudd, A. Valero, A. Valero, Decreasing ore grades in global metallic mining: A theoretical issue or a global reality? *Resources* **5**, 36 (2016).

15. K. D. Kelley, J. R. Lang, R. G. Eppinger, The giant Pebble Cu-Au-Mo deposit and surrounding region, southwest Alaska: Introduction. *Econ. Geol.* **108**, 397–404 (2013).

16. R. A. Padilla Garza, S. R. Titley, F. Pimentel B, Geology of the escondida porphyry copper deposit, antofagasta Region, Chile. *Econ. Geol.* **96**, 307–324 (2001).

17. S. Northey, N. Haque, G. Mudd, Using sustainability reporting to assess the environmental footprint of copper mining. *J. Clean. Prod.* **40**, 118–128 (2013).

18. S. H. Ali, D. Giurco, N. Arndt, E. Nickless, G. Brown, A. Demetriades, R. Durrheim, M. A. Enriquez, J. Kinnaird, A. Littleboy, L. D. Meinert, R. Oberhänsli, J. Salem, R. Schodde, G. Schneider, O. Vidal, N. Yakovleva, Mineral supply for sustainable development requires resource governance. *Nature* **543**, 367–372 (2017).

19. C. Ferreira, P. Jensen, L. Ottosen, A. Ribeiro, Removal of selected heavy metals from MSW fly ash by the electrodialytic process. *Eng. Geol.* **77**, 339–347 (2005).

20. M. R. Jakobsen, J. Fritt-Rasmussen, S. Nielsen, L. M. Ottosen, Electrodialytic removal of cadmium from wastewater sludge. *J. Hazard. Mater.* **106**, 127–132 (2004).

21. Y. B. Acar, A. N. Alshawabkeh, Principles of electrokinetic remediation. *Environ. Sci. Technol.* **27**, 2638–2647 (1993).

22. R. Ortiz-Soto, D. Leal, C. Gutierrez, A. Aracena, A. Rojo, H. K. Hansen, Electrokinetic remediation of manganese and zinc in copper mine tailings. *J. Hazard. Mater.* **365**, 905–911 (2019).

23. R. F. Probstein, R. E. Hicks, Removal of contaminants from soils by electric fields. *Science* **260**, 498–503 (1993).

24. R. H. Sillitoe, Porphyry copper systems. *Econ. Geol.* **105**, 3–41 (2010).

25. L. Sinclair, J. Thompson, In situ leaching of copper: Challenges and future prospects. *Hydrometallurgy* **157**, 306–324 (2015).

26. R. D. Schmidt, D. Earley, M. J. Friedel, *In Situ Recovery of Minerals II. Engineering Foundation*, S. A. Swan, K. R. Coyne, Eds. (TMS, The metals, minerals and materials society, 1994), pp. 259–288.

27. J. E. Dutrizac, Elemental sulphur formation during the ferric chloride leaching of chalcopyrite. *Hydrometallurgy* **23**, 153–176 (1990).

28. G.-N. Kim, D.-B. Shon, H.-M. Park, K.-W. Lee, U.-S. Chung, Development of pilot-scale electrokinetic remediation technology for uranium removal. *Sep. Purif. Technol.* **80**, 67–72 (2011).

29. E. Mena, J. Villaseñor, M. A. Rodrigo, P. Cañizares, Electrokinetic remediation of soil polluted with insoluble organics using biological permeable reactive barriers: Effect of periodic polarity reversal and voltage gradient. *Chem. Eng. J.* **299**, 30–36 (2016).

30. D. Hodges, A. Fourie, D. Thomas, D. Reynolds, Overcoming permanganate stalling during electromigration. *J. Environ. Eng.* **139**, 677–684 (2013).

31. S. S. Kim, S. J. Han, Application of an enhanced electrokinetic ion injection system to bioremediation. *Water Air Soil Pollut.* **146**, 365–377 (2003).

32. C. A. J. Appelo, Solute transport solved with the Nernst-Planck equation for concrete pores with 'free' water and a double layer. *Cem. Concr. Res.* **101**, 102–113 (2017).

33. D. A. Singer, V. I. Berger, B. C. Moring, *Porphyry Copper Deposits of the World: Database, Maps, and Preliminary Analysis* (U.S. Geological Survey, 2002); https://pubs.er.usgs.gov/publication/ofr02268.

34. R. Sprocati, M. Masi, M. Muniruzzaman, M. Rolle, Modeling electrokinetic transport and biogeochemical reactions in porous media: A multidimensional Nernst–Planck–Poisson approach with PHREEQC coupling. *Adv. Water Resour.* **127**, 134–147 (2019).

35. R. Sprocati, M. Rolle, Charge interactions, reaction kinetics and dimensionality effects on electrokinetic remediation: A model-based analysis. *J. Contam. Hydrol.* **229**, 103567 (2020).

36. M. André, M. E. Malmström, I. Neretnieks, Determination of sorption properties of intact rock samples: New methods based on electromigration. *J. Contam. Hydrol.* **103**, 71–81 (2009).

37. M. Löfgren, I. Neretnieks, Through-electromigration: A new method of investigating pore connectivity and obtaining formation factors. *J. Contam. Hydrol.* **87**, 237–252 (2006).

38. E. Puukko, J. Lehto, A. Lindberg, M. Voutilainen, Electromigration experiments for studying transport parameters and sorption of cesium and strontium on intact crystalline rock. *J. Contam. Hydrol.* **217**, 1–7 (2018).

39. R. W. Bartlett, *Solution Mining: Leaching and Fluid Recovery of Minerals* (Routledge, ed. 2, 1998).

40. E. Martens, H. Prommer, X. Dai, J. Sun, P. Breuer, A. Fourie, Electrokinetic in situ leaching of gold from intact ore. *Hydrometallurgy* **178**, 124–136 (2018).

41. M. M. Antonijević, G. D. Bogdanović, Investigation of the leaching of chalcopyritic ore in acidic solutions. *Hydrometallurgy* **73**, 245–256 (2004).

42. C. R. Bennett, D. McBride, M. Cross, J. E. Gebhardt, A comprehensive model for copper sulphide heap leaching: Part 1 Basic formulation and validation through column test simulation. *Hydrometallurgy* **127–128**, 150–161 (2012).

43. N. Hiroyoshi, M. Arai, H. Miki, M. Tsunekawa, T. Hirajima, A new reaction model for the catalytic effect of silver ions on chalcopyrite leaching in sulfuric acid solutions. *Hydrometallurgy* **63**, 257–267 (2002).

44. E. Martens, H. Prommer, X. Dai, M. Z. Wu, J. Sun, P. Breuer, A. Fourie, Feasibility of electrokinetic in situ leaching of gold. *Hydrometallurgy* **175**, 70–78 (2018).

45. D. Hodges, A. Fourie, D. Reynolds, D. Thomas, *Development of An Apparatus for pH-isolated Electrokinetic In Situ Chemical Oxidation. J. Environ. Eng.* **137**, 809–816 (2011).

46. J. Newman, K. E. Thomas-Alyea, *Electrochemical Systems* (John Wiley & Sons, 2004).

47. A. D. MacGillivray, Nernst-Planck equations and the electroneutrality and Donnan equilibrium assumptions. *J. Chem. Phys.* **48**, 2903–2907 (1968).

48. M. Sastre, J. A. Santaballa, A note on the meaning of the electroneutrality condition for solutions. *J. Chem. Educ.* **66**, 403 (1989).

49. B. E. Kimball, J. D. Rimstidt, S. L. Brantley, Chalcopyrite dissolution rate laws. *Appl. Geochem.* **25**, 972–983 (2010).

50. N. N. Saxena, N. R. Mandre, Mixed control kinetics of copper dissolution for copper ore using ferric chloride. *Hydrometallurgy* **28**, 111–117 (1992).

51. C. Y. Cheng, F. Lawson, The kinetics of leaching chalcocite in acidic oxygenated sulphate-chloride solutions. *Hydrometallurgy* **27**, 249–268 (1991).

52. S. Müller, L. Schüler, *GeoStat-Framework/GSTools: Reverberating Red (Version v1.1.0)* (Zenodo, 2019); http://doi.org/10.5281/zenodo.3468230.

53. J. Cai, W. Wei, X. Hu, D. A. Wood, Electrical conductivity models in saturated porous media: A review. *Earth Sci. Rev.* **171**, 419–433 (2017).

54. D. L. Parkhurst, L. Wissmeier, PhreeqcRM: A reaction module for transport simulators based on the geochemical model PHREEQC. *Adv. Water Resour.* **83**, 176–189 (2015).

55. D. R. Lide, *CRC Handbook of Chemistry and Physics* (CRC, London, ed. 84, 2003).

Science Advances

Toward a more sustainable mining future with electrokinetic in situ leaching

Evelien MartensHenning PrommerRiccardo SprocatiJing SunXianwen DaiRich CraneJames JamiesonPablo Ortega TongMassimo RolleAndy Fourie

View the article online
https://www.science.org/doi/10.1126/sciadv.abf9971
Permissions
https://www.science.org/help/reprints-and-permissions

Use of think article is subject to the Terms of service